crystals

MDPI

Article

Dielectric and Piezoelectric Properties of Textured Lead-Free $Na_{0.5}Bi_{0.5}TiO_3$-Based Ceramics

Nannan Dong [1], Xiaoyi Gao [1,2], Fangquan Xia [3], Hanxing Liu [4], Hua Hao [1,*] and Shujun Zhang [2,*]

1 State Key Lab Silicate Materials for Architecture, Center for Smart Materials and Device Integration, School of Materials Science and Engineering, Wuhan University of Technology, Wuhan 430070, China; 18271861079@whut.edu.cn (N.D.); xygao@whut.edu.cn (X.G.)
2 Institute for Superconducting and Electronic Materials, Australian Institute of Innovative Materials, University of Wollongong, NSW 2500, Australia
3 School of Chemistry and Chemical Engineering, University of Jinan, Jinan 250022, China; chm_xiafq@ujn.edu.cn
4 State Key Laboratory of Advanced Technology for Materials Synthesis and Processing, Center for Smart Materials and Device Integration, International School of Materials Science and Engineering, Wuhan University of Technology, Wuhan 430070, China; lhxhp@whut.edu.cn
* Correspondence: haohua@whut.edu.cn (H.H.); shujun@uow.edu.au (S.Z.)

Received: 20 March 2019; Accepted: 12 April 2019; Published: 14 April 2019

Abstract: This work provides a comparative study of the dielectric and piezoelectric properties of randomly oriented and textured $0.88Na_{0.5}Bi_{0.5}TiO_3$-$0.08K_{0.5}Bi_{0.5}TiO_3$-$0.04BaTiO_3$ (88NBT) ceramics. Textured ceramics were fabricated by template grain growth (TGG) method using $NaNbO_3$ (NN) for templates. For textured ceramics with 4 wt% NN templates, a Lotgering factor of 96% and piezoelectric coefficient d_{33} of 185 pC/N were obtained. Compared to the randomly oriented ceramics, textured ceramics show lower strain hysteresis (H = 7.6%), higher unipolar strain of 0.041% with corresponding large signal piezoelectric coefficient d_{33}^* of 200 pm/V at applied field of 2 kV/mm. This enhancement can be explained by the grain orientation along <001> direction by texturing, where an engineered domain configuration is formed after polarization, leading to decreased hysteresis and increased piezoelectric property.

Keywords: textured ceramics; template grain growth; piezoelectric materials; electrical conductivity

1. Introduction

$Na_{0.5}Bi_{0.5}TiO_3$ (NBT) has attracted extensive attention due to their strong ferroelectric properties, with large remnant polarization (P_r = 38 μC/cm^2) and high Curie temperature (T_c = 320 °C) [1]. However, the piezoelectric properties of NBT are inferior to lead based ferroelectric materials, requiring further improvement prior to replacing the lead based counterparts. In the past few decades, several solid solutions have been developed to improve the piezoelectric properties, including $Na_{0.5}Bi_{0.5}TiO_3$-$BaTiO_3$ (NBT-BT) [2–4], $Na_{0.5}Bi_{0.5}TiO_3$-$K_{0.5}Bi_{0.5}TiO_3$ (NBT-KBT) [5,6], $Na_{0.5}Bi_{0.5}TiO_3$-$BaZrO_3$ (NBT-BZT) [7], $Na_{0.5}Bi_{0.5}TiO_3$-$K_{0.5}Bi_{0.5}TiO_3$-$NaNbO_3$ (NBT-KBT-NN) [8], $Na_{0.5}Bi_{0.5}TiO_3$-$K_{0.5}Bi_{0.5}TiO_3$-$BaTiO_3$ (NBT-KBT-BT) [9–13], and $Na_{0.5}Bi_{0.5}TiO_3$-$SrTiO_3$-$BaTiO_3$ (NBT-ST-BT) [14], to name a few.

Many researchers are focusing on the NBT-KBT-BT ternary system, because it provides freedom to tune the compositions to enhance the electromechanical performance, however it sacrifices the temperature stability [9]. Textured method is another approach to improve piezoelectric properties by controlling microstructure and grain orientation, with minimal impact on the Curie temperature T_c. Of particular importance is that the textured ceramics are low cost compared to their single

crystal counterparts [15,16] while exhibiting the anisotropic features similar to single crystal, thus attracting much attention in recent years [16–21]. Enhancements in the piezoelectric d_{33} value of highly textured piezoelectric ceramics have been reported in <001>-textured NBT-BT [16], NBT-KBT [17], NBT-KBT-BT [18], NBT-BT-KNN [19], and $Bi_{1/2}Na_{1/2}TiO_3$-$BaTiO_3$-$AgNbO_3$ (BNT-BT-AN) [20] ceramics, where the effect of templates on dielectric, piezoelectric, and ferroelectric properties of the textured ceramics were discussed. However, the studies on electrical conductivity are limited, which plays an important role in ferroelectric materials since the poling process is impacted by the nature of conductivity of the materials, thus affecting their piezoelectricity. Complex impedance spectroscopy (CIS) is a powerful method to analyze electrical properties, and it has been widely employed to study the conductivity of NBT-based ceramics [22–25].

In this work, $0.88Na_{0.5}Bi_{0.5}TiO_3$-$0.08K_{0.5}Bi_{0.5}TiO_3$-$0.04BaTiO_3$ (88NBT) textured ceramics with morphotropic phase boundary (MPB) composition were prepared by the TGG method. The electrical conductivity, dielectric, piezoelectric, and ferroelectric properties were analyzed in detail.

2. Materials and Methods

<001>-textured 88NBT ceramics were fabricated by TGG using 4 wt % NN templates. NN templates were synthesized by double molten salts synthesis (DMSS). Plate-like layered-perovskite $Bi_{2.5}Na_{3.5}Nb_5O_{18}$ (BNN5) was prepared by a molten synthesis method, using Na_2CO_3 (Sinopharm Chemical Reagent Co. Ltd, Shanghai, China, >99.8%), Nb_2O_5 (Sinopharm Chemical Reagent Co. Ltd, Shanghai, China, 99.99%), and Bi_2O_3 (Aladdin Industrial Corportation, Shanghai, China, 99.9%) as starting powders, with NaCl (Sinopharm Chemical Reagent Co. Ltd, Shanghai, China, 99.5%) as salt (with a weight ratio of oxide to salt at 1:1) [17,26,27]. The mixture was ball milled in ethanol for 24 hours. The dried mixture was placed in a sealed alumina crucible, heated to 1100 °C at a heating rate of 2 °C/min and hold for 4 hours. The resulting mixture was washed several times with hot deionized water to remove the salt until no Cl^- was detected by $AgNO_3$ solution. The synthesized BNN5 particles were then mixed with Na_2CO_3 and equal weight of KCl [28]. After mixing, the mixture was dried for about 24 h, then placed in a sealed alumina crucible. The NN templates were achieved by topo-chemical reaction at 1000 °C for 3 h. Then the crucible was cooled to room temperature with a rate of 5 °C/min. The alumina crucible can be reused many times for fabrication of the templates. After removing the salt, NN templates with a length of ~10μm were synthesized.

We selected $0.88Na_{0.5}Bi_{0.5}TiO_3$-$0.08K_{0.5}Bi_{0.5}TiO_3$-$0.04BaTiO_3$ (88NBT) with MPB composition as the matrix. 88NBT matrix powders were prepared using Bi_2O_3 (Aladdin Industrial Corportation, Shanghai, China, 99.9%), Na_2CO_3 (Sinopharm Chemical Reagent Co. Ltd, Shanghai, China, 99%), TiO_2 (Aladdin Industrial Corportation, Shanghai, China, 99%), K_2CO_3 (Sinopharm Chemical Reagent Co. Ltd, Shanghai, China, 99%), and $BaCO_3$ (Sinopharm Chemical Reagent Co. Ltd, Shanghai, China, 99%) as raw materials by the conventional solid-state reaction method. The powders were ball milled in ethanol for 24 hours, dried, and subsequently calcined at 850 °C for 3 hours. The phase structure was measured by X-ray diffraction (XRD, PANalytical X´ Pert PRO, Eindhoven, The Netherlands). The 88NBT matrix powders were mixed with NN templates, binder, solvents, plasticizers, and dispersant to make slurry, being magnetically stirred for 48 h. The slurry was tape-cast on plastic tape by a doctor blade with a 150 μm gap in height. After drying at room temperature, the green tapes were punched, stacked and laminated at 75 °C with pressure of 50 MPa into disk samples. The green samples were heated to 550 °C with a ramping rate of 1 °C/min and kept for 3 h to burn out the binder and other organic contents. After the burnout process, samples were cold isostatic pressed (CIP) with a pressure of 250 MPa in order to increase the green density and followed by sintering at 1165 °C for 10 h.

The phase structure was measured by X-ray diffraction (XRD, PANalytical X´ Pert PRO, Eindhoven, the Netherlands) and the Lotgering factor was calculated. The samples were poled at 5 kV/mm at room temperature for 15 minutes in a silicone oil bath. The piezoelectric coefficient (d_{33}) was measured by a quasi-static piezoelectric d_{33}-meter (ZJ-3A, Institute of Acoustics, Chinese Academy of Sciences, Beijing, China). Microstructure was examined using a scanning electron microscope (SEM, JSM-7001F,

JEOL, Tokyo, Japan). Dielectric constant (ε) and dielectric loss (tan δ), complex impedance spectra were tested by LCR meter (E4980A, Agilent, Santa Clara, USA) with heating rate of 3 °C/min. The polarization-electric field (*P*–*E*) loops and strain-electric field (*S*–*E*) were measured at 10Hz by a piezo-measurement system (aixACCT TF Analyzer 2000, aixACCT Systems GmbH, Aachen, Germany) with a high voltage amplifier (TREK 610E, Medina, New York, USA).

3. Results and Discussion

Figure 1 shows the XRD pattern and SEM image of the NN templates. The NN templates were prepared from precursor BNN5 particles by the double molten salt method. No other peaks were detected, indicating that a pure perovskite $NaNbO_3$ phase was obtained. All the NN particles have a plate-like shape with a length of 5~10 μm and average thickness of 0.5~1 μm. This large aspect ratio is expected to benefit the fabrication of textured ceramics by tape-casting technology [29].

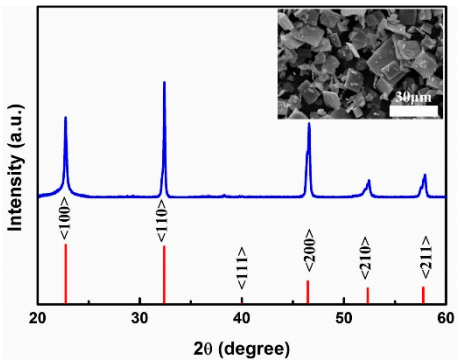

Figure 1. XRD pattern of $NaNbO_3$ templates; the inset shows an SEM image of the $NaNbO_3$ templates.

Figure 2a shows the XRD patterns of 88NBT randomly oriented ceramics and textured ceramics. No impurity phase was detected, suggesting the samples were in pure perovskite structure. It is noticed that the most intensive peak is <110> in randomly oriented ceramics, while the <100> and <200> peaks increase rapidly with significantly reduced non-<l00> peaks for the 88NBT textured ceramics, demonstrating a strongly-preferred grain orientation of the 88NBT textured ceramics along the <l00> direction. The <200> peak located at 46° splits into <200>/<002>, suggesting the coexistence of the rhombohedral phase and tetragonal phase. The Lotgering factor (*F*) was calculated from the XRD pattern in the range of 20°–60° by the formula [30]

$$F = \frac{P - P_0}{1 - P_0} \tag{1}$$

where P and P_0 are $\sum I_{(h00)} / \sum I_{(hkl)}$ in the textured and randomly oriented ceramics, respectively.

The Lotgering factor of the textured sample was found to be approximately 96%. This result shows that the high degree of the textured 88NBT ceramics can be obtained using the plate-like NN templates by optimizing the fabrication process. The SEM images of matrix powders, randomly oriented and textured ceramics are shown in Figure 2b–d, respectively. The prepared powders with a small average size of about 100 nm are shown in Figure 2b, which will benefit the textured ceramic fabrication due to the smaller particle size in the matrix powders will provide a greater driving force of nucleation along the preferred orientation [31]. As shown in Figure 2c, the grain size of the randomly-oriented ceramics is about 1 μm. In contrast, the textured ceramics are observed to possess the brick-like shape with a larger grain size being on the order of 8 μm, as shown in Figure 2d. The density of both samples is measured by the Archimedes' method. The relative density of the textured 88NBT ceramic is found to be 95% while that of the randomly oriented ceramics is 96%.

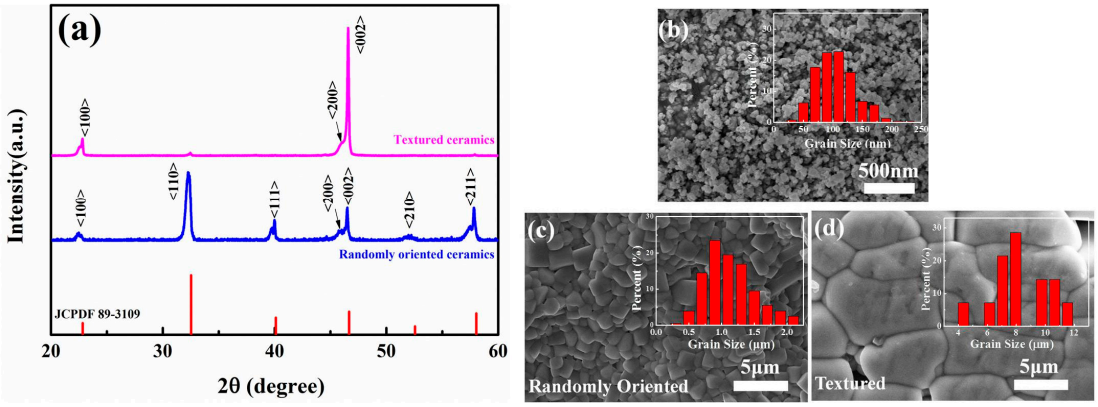

Figure 2. (**a**) XRD patterns of 88NBT randomly oriented ceramics and textured ceramics. SEM images of 88NBT (**b**) matrix powders; (**c**) randomly oriented ceramics; (**d**) textured ceramics. The insets give the grain size distributions.

Temperature-dependent dielectric constant and loss for 88NBT ceramics at different frequencies are shown in Figure 3, exhibiting two obvious dielectric anomalies in the dielectric constant: T_d (depolarization temperature) and T_m (temperature of the maximum dielectric constant). T_d refers to the temperature of the transition between ferroelectric phase and anti-ferroelectric phase, or polar state to non-polar state, while T_m stands for the temperature of the transition between anti-ferroelectric phase and paraelectric phase [32]. The T_d and T_m are found to be ~120 °C and ~290 °C for the randomly oriented ceramics, respectively, while the textured ceramics are found to possess slightly lower T_d (~110 °C) and T_m (~270 °C). This phenomenon is attributed to the residual internal stresses from the template grains, a slight composition deviation, and the integrated aging effect in the textured ceramics [19,20,33]. The dielectric constant at room temperature ($\varepsilon_{25\,°C}$) for the randomly-oriented ceramics is about 800, whereas the $\varepsilon_{25°C}$ for textured ceramics is 810 (at 10 kHz). On the contrary, the maximum dielectric constant ε_{max} of the randomly oriented ceramics is 5350, decreased significantly to ~3950 for textured ceramics, where less extrinsic contribution is thought to be the main reason for the depressed dielectric maxima in the textured ceramics, while the higher residual pore concentration in the textured ceramics may also impact the crystallinity and maximum dielectric constant [19,34]. With the ε_{max} decreased, the textured ceramics show temperature stable dielectric behavior over a broad temperature range.

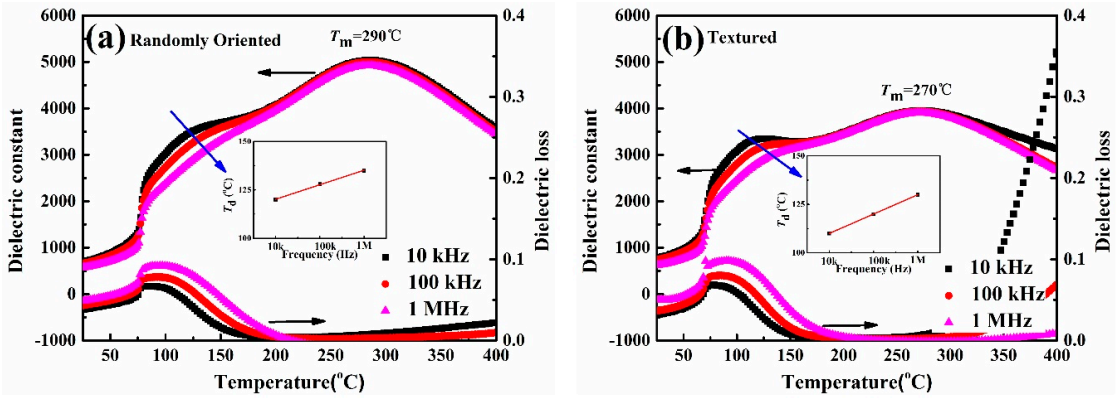

Figure 3. Temperature dependence of dielectric constant and dielectric loss of (**a**) 88NBT randomly oriented ceramics and (**b**) 88NBT textured ceramics. The insets give the frequency dependent T_d.

The randomly-oriented and textured 88NBT ceramics exhibit broad dielectric peaks around T_m and frequency dependent dielectric near the T_d temperature, reflecting the diffuse phase transition

behavior, which is believed to be associated with the coexistence of complex cations (Na^+, Bi^{3+}, K^+ and Ba^{2+}) on A-site [35]. The relaxor behavior can be described by the modified Curie–Weiss law [36]

$$\frac{1}{\varepsilon} - \frac{1}{\varepsilon_{max}} = \frac{(T - T_m)^\gamma}{C} \quad (2)$$

where ε is the dielectric constant, ε_{max} is the dielectric constant at T_m, C is the Curie constant, and γ is the degree of diffuseness in the range of 1–2. The $\gamma = 1$ represents a normal ferroelectric and $\gamma = 2$ stands for an ideal ferroelectric relaxor. The value of γ is calculated from the slope of $\ln(1/\varepsilon - 1/\varepsilon_m)$ versus $\ln(T\text{-}T_m)$ plot at 100 kHz, as shown in Figure 4. The γ of the randomly oriented ceramics is 1.896, slightly increases to 1.917 for the 88NBT textured ceramics, implying the introducing of Nb^{5+} cations on B site due to the NN template will also contribute to the relaxor behavior.

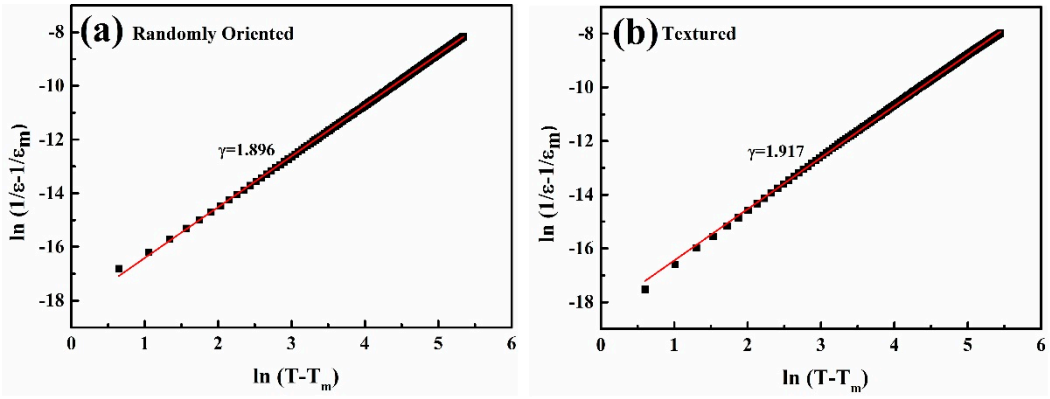

Figure 4. The plot of $\ln(1/\varepsilon - 1/\varepsilon_m)$ as a function of $\ln(T\text{-}T_m)$ for (**a**) 88NBT randomly oriented ceramics and (**b**) 88NBT textured ceramics at 100 kHz.

Figure 5 gives the complex impedance (Z*) plots for randomly oriented and textured 88NBT ceramics over the temperatures range of 340–500 °C. All the plots at different temperatures show similar behaviors. In the complex impedance plots, the low frequency intercept of the impedance data on the real axis Z' corresponds to the bulk resistance. An equivalent circuit with two parallel R-C elements is adopted to fit the experimental data, as shown in Figure 5c. The resistance and capacitance components of the grains are labeled as R1 and C1, the resistance and capacitance components of the grain boundaries are labeled as R2 and C2. Based on the equivalent circuit, the resistances (R) and capacitances (C) of grains and grain boundaries can be calculated by Z-View software. Table 1 lists the fitted parameters of the randomly-oriented and textured ceramics.

Table 1. Electrical parameters of randomly oriented and textured ceramics.

Temperature (°C)	Randomly-Oriented		Textured	
	R_1 (kΩ)	R_2 (MΩ)	R_1 (kΩ)	R_2 (MΩ)
500	12.8	0.2	24.9	0.07
480	18.1	0.25	45.0	0.13
460	25.3	0.35	69.4	0.18
440	33.6	0.66	93.23	0.22
420	57.1	1.33	108.9	0.24
400	65.8	3.66	113.9	0.40
380	66.2	8.41	127.0	0.79
360	68.5	14.3	149.4	2.7
340	73.5	24.3	168.2	9.2

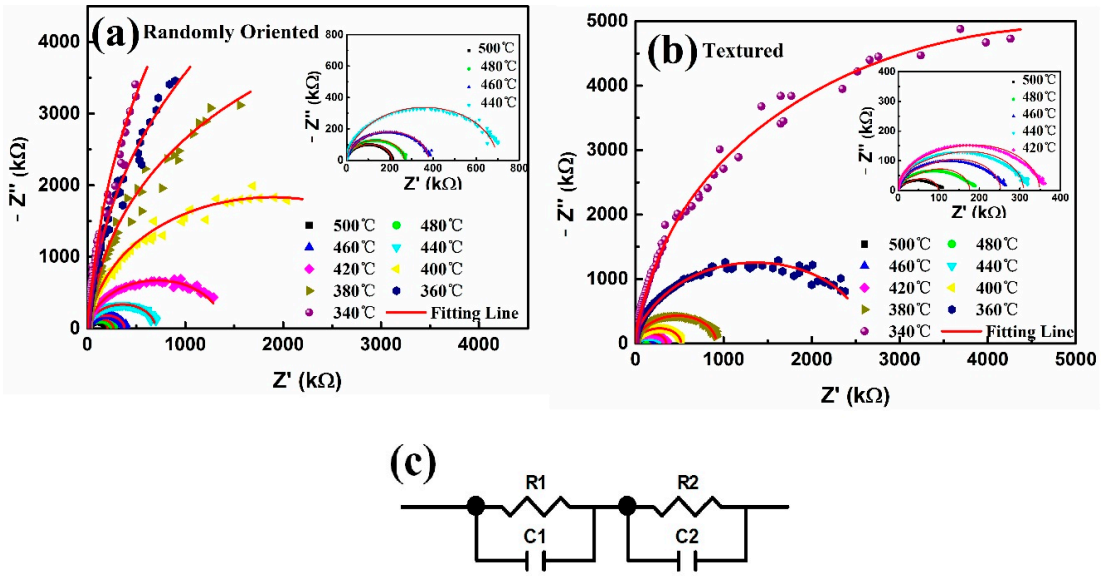

Figure 5. Complex impedance plots of 88NBT randomly oriented and textured ceramics at different measuring temperatures (**a**–**c**). Equivalent circuit proposed for 88NBT ceramics, R_1, R_2, C_1, and C_2 are the resistances and capacitances of grains and grain boundaries, respectively.

The *ac* conductivity is obtained in accordance with the literature [37]. Figure 6a,b show the plot of *ac* conductivity (σ_{ac}) versus frequency at different temperatures. At low frequency, the conductivity keeps almost constant, while in high frequency region, conductivity increases with frequency. The *ac* conductivity data in Figure 6a,b obey the Jonscher's power law [38,39]. Compared to the randomly-oriented ceramics, textured ceramics show higher *ac* conductivity. Figure 6c represents the variation of *dc* conductivity with inverse of absolute temperature for randomly oriented and textured ceramics, in which the *dc* conductivity values are obtained from non-linear fitting of the *ac* conductivity curves using Jonscher's power law. The σ_{dc} can be explained by the empirical relation [40]

$$\sigma_{dc} = \sigma_0 \exp(-E_a/k_B T) \quad (3)$$

where σ_0 is pre exponential factor, E_a is the activation energy of conduction, k_B is the Boltzmann constant, and T is the absolute temperature. The E_a of the 88NBT randomly oriented ceramics is calculated to be 1.49 eV, which is close to the reported data for NBT based ceramics [24,41,42]. The value of E_a is approximately half the band gap (3.25–3.4 eV) of NBT-BT materials [43], indicating that the 88NBT randomly oriented ceramics exhibit electronic conductive behavior that is closely related to intrinsic band-type conduction [24,41]. Compared to the 88NBT randomly oriented ceramics, the 88NBT textured ceramics possess lower E_a, being on the order of 1.13 eV, which may relate to the increased grain size as well as the lower grain boundary density.

Figure 7a exhibits polarization-electric field (*P*-*E*) loops for textured and randomly oriented 88NBT ceramics measured at 7 kV/mm and 1 Hz. The ferroelectric properties of the textured and randomly oriented ceramics are summarized in Table 2. The remnant polarizations P_r of randomly-oriented and textured ceramics are 35.2 and 26.4 μC/cm^2, respectively, with coercive fields E_c being on the order of 3.5 and 3.1 kV/mm, respectively. The textured ceramics show lower coercive field and remnant polarization. The lower coercive field of the textured ceramics is believed to be associated with the larger grain comparing to randomly oriented one, as observed in Figure 2c,d, where far fewer grain boundaries will make the ferroelastic domain wall reversal easier. Figure 7b shows the bipolar strain curves (*S*–*E* curves) of randomly-oriented and textured ceramics. Both the *S*–*E* curves display a typical butterfly shape, where the *E* field-induced strains at 7 kV/mm in randomly and textured 88NBT ceramics are 0.15% and 0.19%, respectively. In order to understand the strain behavior more clearly, the unipolar strain curves were also measured and given in Figure 7c. The strain response of the randomly

oriented ceramics is about ~0.032% at 2 kV/mm, while the maximum strain of S_{max}~0.041% is observed for the textured ceramics at the same electric field level. The large signal piezoelectric coefficient d_{33}^* and strain hysteresis H can be calculated according to the formula [44]

$$d_{33}^* = S_{max}/E_{max} \quad (4)$$

$$H = \frac{H_{E_{max/2}}}{S_{max}} \quad (5)$$

The d_{33}^* are 160 and 200 pm/V for the randomly-oriented and textured ceramics at 2 kV/mm, respectively, where the d_{33}^* of the textured ceramics possess ~25% enhancement comparing to randomly oriented one. Of particular significance is that the strain hysteresis of the randomly oriented ceramics is 16%, greatly decreases to 7.6% for the textured 88NBT ceramics. This phenomena can be explained by the texturing characteristics, where all the grains in the textured ceramics are aligned along crystallographic <001> direction, analogous to <001> poled single crystals [45], a specific domain engineered configuration is expected to exist in the <001> poled textured ceramics, being responsible for the enhanced piezoelectric coefficient. Meanwhile, the reduced hysteresis observed in textured 88NBT ceramics is similar to the dielectric nonlinearity reported in the textured KNN ceramics, where the pre-orientation of domain configuration in the <001> texture ceramics is responsible for the reduction [46–49], in addition to the enlarged grain size (thus increased domain size and decreased domain wall density).

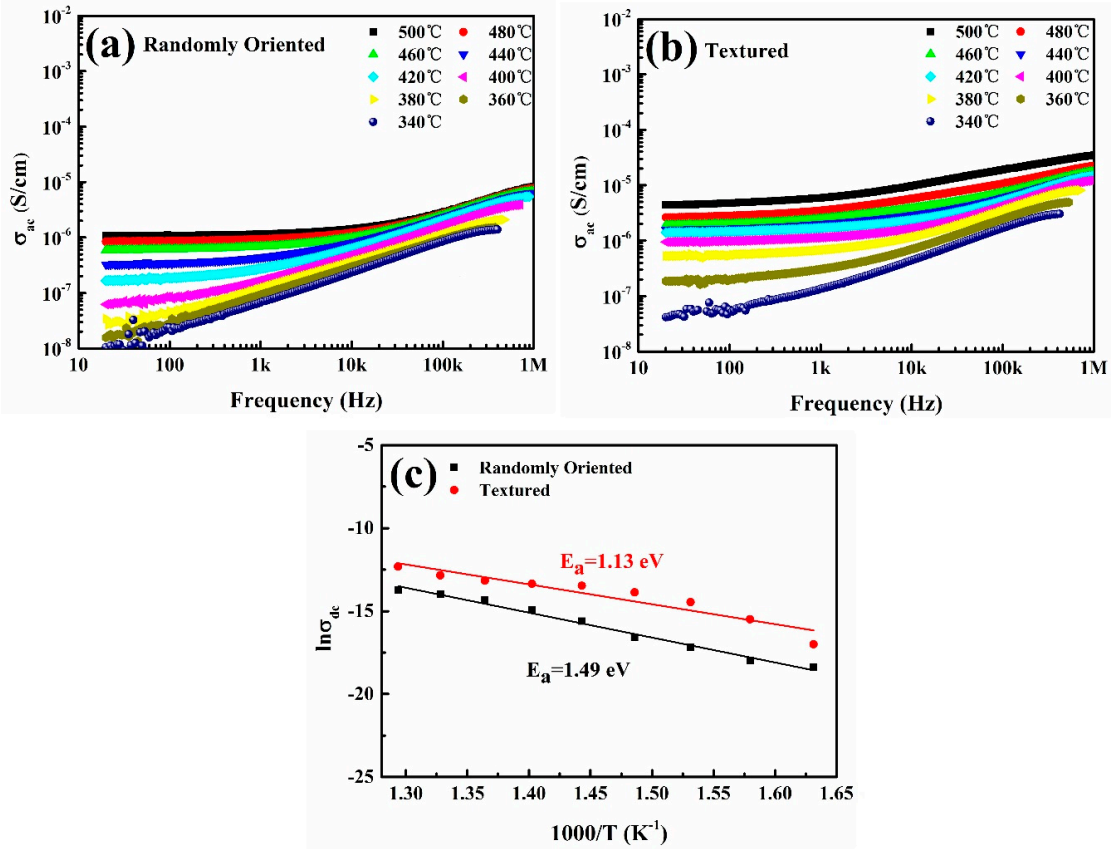

Figure 6. Frequency dependence of *ac* conductivity for (**a**) randomly-oriented and (**b**) textured ceramics as a function of temperature. (**c**) Temperature dependence *dc* conductivity (σ_{dc}) for 88NBT randomly and textured ceramics.

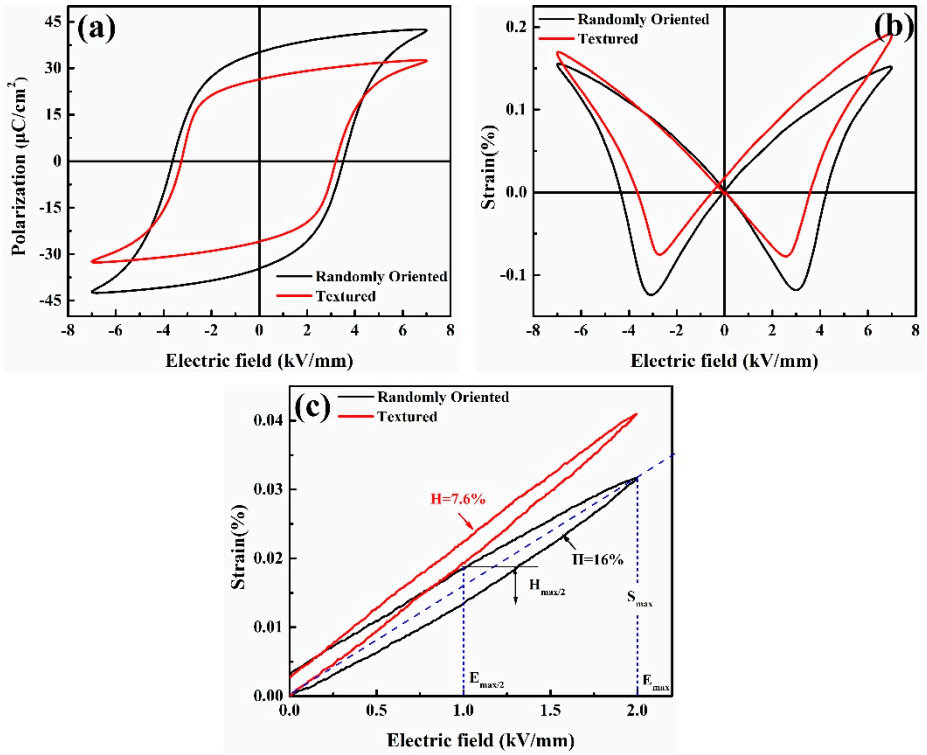

Figure 7. (**a**) Polarization hysteresis loops, (**b**) bipolar strain curves, and (**c**) unipolar strain curves for randomly oriented and textured 88NBT ceramics.

Table 2. Piezoelectric, dielectric, and ferroelectric properties of 88NBT randomly oriented and textured ceramics.

Sample	P_r (μC/cm²)	E_c (kV/mm)	S_{max}	H	d_{33} * (pm/V)	d_{33} (pC/N)	T_d (°C)	T_m (°C)	$\varepsilon_{25\,°C}$ (at 10 kHz)	ε_{max} (at 10 kHz)	tanδ (25 °C)
Random	35.2	3.5	0.032%	16%	160	150	120	290	800	5350	0.038
Textured	26.4	3.1	0.041%	7.6%	200	185	110	270	810	3950	0.032

Note: d_{33}^* denotes the large signal piezoelectric coefficient of ceramics.

4. Conclusions

In conclusion, highly textured $0.88Na_{0.5}Bi_{0.5}TiO_3$-$0.08K_{0.5}Bi_{0.5}TiO_3$-$0.04BaTiO_3$ ceramics with Lotgering factor F = 96% were fabricated by the TGG method using NN as templates. The large signal d_{33}^* value at 2 kV/mm is found to be on the order of 200 pm/V for the textured ceramic, a 25% enhancement when compared to the randomly-oriented counterpart. In addition, the strain hysteresis is about 7.6% for textured ceramics, being half the value of the hysteresis in randomly oriented counterpart. These results demonstrate that the texturing method is an effective way to enhance the piezoelectric properties by controlling grain alignment and microstructure.

Author Contributions: Material fabrication and property characterization, N.D. and X.G.; Writing—original draft, N.D.; Writing—review and editing, N.D., X.G., F.X., H.H., H.L., and S.Z.

Funding: This research was funded by NSFC-Guangdong Joint Funds of the Natural Science Foundation of China (no. U1601209), Major Program of the Natural Science Foundation of China (51790490) and the Technical Innovation Program of Hubei Province (grant no. 2017AHB055).

Conflicts of Interest: The authors declare no conflict of interest.

References

1. Smolenskii, G.A.; Isupov, V.A.; Agranovskaya, A.I.; Krainik, N.N. New Ferroelectrics of Complex Composition. *Sov. Phys. Solid State* **1961**, *2*, 2651–2654.
2. Xu, Q.; Chen, X.-L.; Chen, W.; Chen, M.; Xu, S.-L.; Kim, B.-H.; Lee, J.-H. Effect of MnO addition on structure and electrical properties of $(Na_{0.5}Bi_{0.5})_{0.94}Ba_{0.06}TiO_3$ ceramics prepared by citrate method. *Mater. Sci. Eng. B* **2006**, *130*, 94–100. [CrossRef]
3. Chen, M.; Xu, Q.; Kim, B.H.; Ahn, B.K.; Ko, J.H.; Kang, W.J.; Nam, O.J. Structure and electrical properties of $(Na_{0.5}Bi_{0.5})_{1-x}Ba_xTiO_3$ piezoelectric ceramics. *J. Eur. Ceram. Soc.* **2008**, *28*, 843–849. [CrossRef]
4. Hajra, S.; Sahoo, S.; Das, R.; Choudhary, R.N.P. Structural, dielectric and impedance characteristics of $(Bi_{0.5}Na_{0.5})TiO_3$-$BaTiO_3$ electronic system. *J. Alloys Compd.* **2018**, *750*, 507–514. [CrossRef]
5. Otonicar, M.; Park, J.; Logar, M.; Esteves, G.; Jones, J.L.; Jancar, B. External-field-induced crystal structure and domain texture in $(1-x)Na_{0.5}Bi_{0.5}TiO_{3-x}K_{0.5}Bi_{0.5}TiO_3$ piezoceramics. *Acta Mater.* **2017**, *127*, 319–331. [CrossRef]
6. Muneeswaran, M.; Choi, B.C.; Chang, S.H.; Jung, J.H. Effect of dysprosium doping on structural and vibrational properties of lead-free $(Na_{0.7}K_{0.3})_{0.5}Bi_{0.5}TiO_3$ ferroelectric ceramics. *Ceram. Int.* **2017**, *43*, 13696–13701. [CrossRef]
7. Hussain, A.; Rahman, J.U.; Maqbool, A.; Kim, M.S.; Song, T.K.; Kim, W.J.; Kim, M.H. Structural and electromechanical properties of lead-free $Na_{0.5}Bi_{0.5}TiO_3$-$BaZrO_3$ ceramics. *Phys. Status Solidi A* **2014**, *211*, 1704–1708. [CrossRef]
8. Xu, Q.; Lanagan, M.T.; Luo, W.; Zhang, L.; Xie, J.; Hao, H.; Cao, M.H.; Yao, Z.H.; Liu, H.X. Electrical properties and relaxation behavior of $Bi_{0.5}Na_{0.5}TiO_3$-$BaTiO_3$ ceramics modified with $NaNbO_3$. *J. Eur. Ceram. Soc.* **2016**, *36*, 2469–2477. [CrossRef]
9. Zhang, S.; Shrout, T.R.; Nagata, H.; Hiruma, Y.; Takenaka, T. Piezoelectric properties in $(K_{0.5}Bi_{0.5})TiO_3$-$(Na_{0.5}Bi_{0.5})TiO_3$-$BaTiO_3$ lead-free ceramics. *IEEE Trans. Ultrason. Ferroelectr. Freq. Control* **2007**, *54*, 910–917. [CrossRef] [PubMed]
10. Li, Y.; Chen, W.; Xu, Q.; Zhou, J.; Gu, X. Piezoelectric and ferroelectric properties of $Na_{0.5}Bi_{0.5}TiO_3$-$K_{0.5}Bi_{0.5}TiO_3$-$BaTiO_3$ piezoelectric ceramics. *Mater. Lett.* **2005**, *59*, 1361–1364. [CrossRef]
11. Liu, G.; Jiang, W.; Zhang, L.; Cai, J.; Wang, Z.; Liu, K.; Liu, X.; Chen, Y.; Liu, H.; Yan, Y. Effects of sintering temperature and KBT content on microstructure and electrical properties of $(Bi_{0.5}Na_{0.5})TiO_3$-$BaTiO_3$-$(Bi_{0.5}K_{0.5})TiO_3$ Pb-free ceramics. *Ceram. Int.* **2018**, *44*, 9303–9311. [CrossRef]
12. Zhang, S.-T.; Yang, B.; Cao, W. The temperature-dependent electrical properties of $Bi_{0.5}Na_{0.5}TiO_3$-$BaTiO_3$-$Bi_{0.5}K_{0.5}TiO_3$ near the morphotropic phase boundary. *Acta Mater.* **2012**, *60*, 469–475. [CrossRef]
13. Li, Y.; Zhang, Y.; Sun, H.; Liu, X.; Sui, H.; Zhou, D.; Guo, Q. Phase structure and electrical properties of lead-free (1−2x)NBT-xKBT-xBT ceramics. *J. Mater. Sci. Mater. Electron.* **2018**, *29*, 7851–7856. [CrossRef]
14. Praharaj, S.; Subramanian, V.; Kang, S.J.L.; Rout, D. Origin of relaxor behavior in $0.78(Na_{0.5}Bi_{0.5})TiO_3$-$0.2SrTiO_3$-$0.02BaTiO_3$ ceramic: An electrical modulus study. *Mater. Res. Bull.* **2018**, *106*, 459–464. [CrossRef]
15. Moriana, A.D.; Zhang, S. Lead-free textured piezoceramics using tape casting: A review. *J. Mater.* **2018**, *4*, 277–303. [CrossRef]
16. Maurya, D.; Zhou, Y.; Yan, Y.; Priya, S. Synthesis mechanism of grain-oriented lead-free piezoelectric $Na_{0.5}Bi_{0.5}TiO_3$-$BaTiO_3$ ceramics with giant piezoelectric response. *J. Mater. Chem. C* **2013**, *1*, 2102–2111. [CrossRef]
17. Bai, W.; Chen, D.; Zheng, P.; Xi, J.; Zhou, Y.; Shen, B.; Zhai, J.; Ji, Z. $NaNbO_3$ templates-induced phase evolution and enhancement of electromechanical properties in <001> grain oriented lead-free BNT-based piezoelectric materials. *J. Eur. Ceram. Soc.* **2017**, *37*, 2591–2604. [CrossRef]
18. Maurya, D.; Zhou, Y.; Wang, Y.; Yan, Y.; Li, J.; Viehland, D.; Priya, S. Giant strain with ultra-low hysteresis and high temperature stability in grain oriented lead-free $K_{0.5}Bi_{0.5}TiO_3$-$BaTiO_3$-$Na_{0.5}Bi_{0.5}TiO_3$ piezoelectric materials. *Sci. Rep.* **2015**, *5*, 8595. [CrossRef]
19. Ma, S.; Zhang, Y.; Liu, Z.; Dai, X.; Huang, J.; Fan, P.; Xie, B.; Jiang, S.; Zhang, H. Preparation and enhanced electric-field-induced strain of textured 91BNT-6BT-3KNN lead-free piezoceramics by TGG method. *J. Mater. Sci. Mater. Electron.* **2015**, *27*, 3076–3081. [CrossRef]

20. Zhang, H.; Xu, P.; Patterson, E.; Zang, J.; Jiang, S.; Rödel, J. Preparation and enhanced electrical properties of grain-oriented $(Bi_{1/2}Na_{1/2})TiO_3$-based lead-free incipient piezoceramics. *J. Eur. Ceram. Soc.* **2015**, *35*, 2501–2512. [CrossRef]
21. Bai, W.; Chen, D.; Zheng, P.; Zhang, J.; Shen, B.; Zhai, J.; Ji, Z. Low electric field-driven giant strain response in <001> textured BNT-based lead-free piezoelectric materials. *J. Mater. Sci.* **2016**, *52*, 3169–3178. [CrossRef]
22. Chandrasekhar, M.; Khatua, D.K.; Pattanayak, R.; Kumar, P. Dielectric relaxation and conduction mechanism studies of BNT-BT-BKT ceramics. *J. Phys. Chem. Solids* **2017**, *111*, 160–166. [CrossRef]
23. Bongkarn, T.; Cann, D.P.; Prasertpalichat, S.; Kumar, N.; Sumang, R. Impedance spectroscopy of lead-free $(1-x-y)Bi_{0.5}Na_{0.5}TiO_3-xBi_{0.5}K_{0.5}TiO_3-yBi_{0.5}Li_{0.5}TiO_3$ piezoelectric ceramics. *Integr. Ferroelectr.* **2017**, *177*, 79–89. [CrossRef]
24. Xu, Q.; Lanagan, M.T.; Huang, X.C.; Xie, J.; Zhang, L.; Hao, H.; Liu, H.X. Dielectric behavior and impedance spectroscopy in lead-free BNT-BT-NBN perovskite ceramics for energy storage. *Ceram. Int.* **2016**, *42*, 9728–9736. [CrossRef]
25. Zidi, N.; Chaouchi, A.; d'Astorg, S.; Rguiti, M.; Courtois, C. Dielectric and impedance spectroscopy characterizations of CuO added $(Na_{0.5}Bi_{0.5})_{0.94}Ba_{0.06}TiO_3$ lead-free piezoelectric ceramics. *J. Alloys Compd.* **2014**, *590*, 557–564. [CrossRef]
26. Yan, Y.; Liu, D.; Zhao, W.; Zhou, H.; Fang, H. Topochemical synthesis of a high-aspect-ratio platelet NaNbO3 template. *J. Am. Ceram. Soc.* **2007**, *90*, 2399–2403. [CrossRef]
27. Zhang, M.; Fan, H.; Chen, L.; Yang, C. Synthesis and formation mechanisms of high aspect ratio platelike $NaNbO_3$ particles by topochemical microcrystal conversion. *J. Alloys Compd.* **2009**, *476*, 847–853. [CrossRef]
28. Li, L.; Zhang, Y.; Bai, W.; Shen, B.; Zhai, J.; Chen, H. Synthesis of high aspect ratio $(K,Na)NbO_3$ plate-like particles and study on the synthesis mechanism. *Dalton Trans.* **2015**, *44*, 11621–11625. [CrossRef]
29. Zhao, W.; Ya, J.; Xin, Y.; Lie, E.; Zhao, D.; Zhou, H. Fabrication of $Na_{0.5}Bi_{0.5}TiO_3$-$BaTiO_3$-Textured Ceramics Templated by Plate-Like $Na_{0.5}Bi_{0.5}TiO_3$ Particles. *J. Am. Ceram. Soc.* **2009**, *92*, 1607–1609. [CrossRef]
30. Lotgering, F.K. Topotactical reactions with ferrimagnetic oxides having hexagonal crystal structures-I. *J. Inorg. Nucl. Chem.* **1959**, *9*, 113–123. [CrossRef]
31. Messing, G.L.; Trolier-McKinstry, S.; Sabolsky, E.M.; Duran, C.; Kwon, S.; Brahmaroutu, B.; Park, P.; Yilmaz, H.; Rehrig, P.W.; Eitel, K.B.; et al. Templated Grain Growth of Textured Piezoelectric Ceramics. *Crit. Rev. Solid State Mater. Sci.* **2004**, *29*, 45–96. [CrossRef]
32. Deng, M.; Li, X.; Zhao, Z.; Li, T.; Dai, Y.; Ji, H. Crystallographic textured evolution in $0.85Na_{0.5}Bi_{0.5}TiO_3$-$0.04BaTiO_3$-$0.11K_{0.5}Bi_{0.5}TiO_3$ ceramics prepared by reactive-templated grain growth method. *J. Mater. Sci. Mater. Electron.* **2014**, *25*, 1873–1879. [CrossRef]
33. Bai, W.; Wang, L.; Zheng, P.; Wen, F.; Zhai, J.; Ji, Z. Pairing high piezoelectric properties and enhanced thermal stability in grain-oriented BNT-based lead-free piezoceramics. *Ceram. Int.* **2018**, *44*, 11402–11409. [CrossRef]
34. Bai, W.; Li, H.; Xi, J.; Zhang, J.; Shen, B.; Zhai, J. Effect of different templates and texture on structure evolution and strain behavior of <001>-textured lead-free piezoelectric BNT-based ceramics. *J. Alloys Compd.* **2016**, *656*, 13–23. [CrossRef]
35. Chen, X.; Ma, H.; Pan, W.; Pang, M.; Liu, P.; Zhou, J. Microstructure, dielectric and ferroelectric properties of $(Na_xBi_{0.5})_{0.94}Ba_{0.06}TiO_3$ lead-free ferroelectric ceramics: Effect of Na nonstoichiometry. *Mater. Chem. Phys.* **2012**, *132*, 368–374. [CrossRef]
36. Wei, M.; Zhang, J.; Zhang, M.; Yao, Z.; Chen, H.; Yang, C. Relaxor behavior of $BaTiO_3$-$BiYO_3$ perovskite materials for high energy density capacitors. *Ceram. Int.* **2017**, *43*, 4768–4774. [CrossRef]
37. Rani, R.; Sharma, S.; Rai, R.; Kholkin, A.L. Dielectric behavior and impedance analysis of lead-free CuO doped $(Na_{0.50}K_{0.50})_{0.95}(Li_{0.05}Sb_{0.05}Nb_{0.95})O_3$ ceramics. *Solid State Sci.* **2013**, *17*, 46–53. [CrossRef]
38. Kim, J.S.; Hussain, A.; Kim, M.-H.; Song, T.K.; Chung, S.T.; Chung, C.H.; Lee, H.S. Dielectric and conduction behaviors of lead-free $LiNbO_3$-modified $Bi_{0.5}Na_{0.5}TiO_3$ ceramics. *J. Korean Phys. Soc.* **2012**, *61*, 951–955. [CrossRef]
39. Roy, A.K.; Singh, A.; Kumari, K.; Amar Nath, K.; Prasad, A.; Prasad, K. Electrical Properties and AC Conductivity of $(Bi_{0.5}Na_{0.5})_{0.94}Ba_{0.06}TiO_3$ Ceramic. *ISRN Ceram.* **2012**, *2012*, 1–10. [CrossRef]
40. Moure, A.; Pardo, L. Microstructure and texture dependence of the dielectric anomalies and dc conductivity of Bi_3TiNbO_9 ferroelectric ceramics. *J. Appl. Phys.* **2005**, *97*, 084103. [CrossRef]
41. Zang, J.; Li, M.; Sinclair, D.C.; Jo, W.; Rödel, J.; Zhang, S. Impedance Spectroscopy of $(Bi_{1/2}Na_{1/2})TiO_3$-$BaTiO_3$ Ceramics Modified with $(K_{0.5}Na_{0.5})NbO_3$. *J. Am. Ceram. Soc.* **2014**, *97*, 1523–1529. [CrossRef]

42. East, J.; Sinclair, D.C. Characterization of $(Bi_{1/2}Na_{1/2})TiO_3$ using electric modulus spectroscopy. *J. Mater. Sci. Lett.* **1997**, *16*, 422–425. [CrossRef]
43. Cernea, M.; Galca, A.C.; Cioangher, M.C.; Dragoi, C.; Ioncea, G. Piezoelectric BNT-$BT_{0.11}$ thin films processed by sol-gel technique. *J. Mater. Sci.* **2011**, *46*, 5621–5627. [CrossRef]
44. Kungl, H.; Fett, T.; Wagner, S.; Hoffmann, M.J. Nonlinearity of strain and strain hysteresis in morphotropic LaSr-doped lead zirconate titanate under unipolar cycling with high electric fields. *J. Appl. Phys.* **2007**, *101*, 044101. [CrossRef]
45. Zhang, S.; Li, F. High performance ferroelectric relaxor-$PbTiO_3$ single crystals: Status and perspective. *J. Appl. Phys.* **2012**, *111*, 031301. [CrossRef]
46. Haugen, A.B.; Morozov, M.I.; Jones, J.L.; Einarsrud, M.-A. Rayleigh analysis of dielectric properties in textured $K_{0.5}Na_{0.5}NbO_3$ ceramics. *J. Appl. Phys.* **2014**, *116*, 214101. [CrossRef]
47. Huan, Y.; Wang, X.; Li, L.; Koruza, J. Strong domain configuration dependence of the nonlinear dielectric response in (K,Na)NbO_3-based ceramics. *Appl. Phys. Lett.* **2015**, *107*, 202903. [CrossRef]
48. Li, P.; Zhai, J.; Shen, B.; Zhang, S.; Li, X.; Zhu, F.; Zhang, X. Ultrahigh piezoelectric properties in textured (K,Na)NbO_3 -based lead-free ceramics. *Adv. Mater.* **2018**, *30*, 1705171. [CrossRef] [PubMed]
49. Liu, B.; Li, P.; Shen, B.; Zhai, J.; Zhang, Y.; Li, F.; Liu, X. Enhanced piezoelectric properties and temperature-insensitive strain behavior of <001>-textured KNN-based ceramics. *Ceram. Int.* **2017**, *43*, 8004–8009. [CrossRef]